International Journal of Biological Macromolecules 283 (2024) 137691

Contents lists available at ScienceDirect

International Journal of Biological Macromolecules

journal homepage: www.elsevier.com/locate/ijbiomac

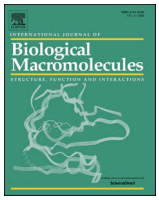

Deciphering the role of neutral diruthenium complexes in protein binding☆

Giarita Ferraro [a], Aarón Terán [b], Francesco Galardo [a], Rosanna Lucignano [a], Delia Picone [a], Lara Massai [c], Francesca Fasulo [b], Ana B. Muñoz-García [b], Luigi Messori [c], Santiago Herrero [d,e], Antonello Merlino [a,*]

[a] Department of Chemical Sciences, University of Naples Federico II, Complesso Univ. di Monte Sant'Angelo, via Cinthia, 26, 80126 Naples, Italy
[b] Department of Physics "Ettore Pancini", University of Naples Federico II, Complesso Univ. di Monte Sant'Angelo, via Cinthia, 26, 80126 Naples, Italy
[c] Department of Chemistry "Ugo Schiff", University of Florence, via della Lastruccia 3-13, 50019, Sesto Fiorentino, Florence, Italy
[d] MatMoPol Research Group, Department of Inorganic Chemistry, Faculty of Chemical Sciences, Complutense University of Madrid, Avda. Complutense s/n, 28040, Madrid, Spain
[e] Knowledge Technology Institute, Complutense University of Madrid, Campus de Somosaguas, 28223, Pozuelo de Alarcón, Madrid, Spain

A B S T R A C T

The charge of paddlewheel diruthenium complexes has a major role in defining their interaction with proteins: negatively charged complexes bind proteins non-covalently, while cationic complexes form adducts where the Ru_2 core binds to Asp side chains at the equatorial sites, or to the main chain carbonyl groups or the side chains of His, Arg or Lys residues at the axial sites. Here we study the interactions of the neutral compound $[Ru_2(D\text{-}p\text{-}FPhF)(O_2CCH_3)_2(O_2CO)]\cdot 3H_2O$ (D-*p*-$FPhF^- = N,N'$-*bis*(4-fluorophenyl)formamidinate), a very rare example of a paddlewheel diruthenium compound with three different equatorial ligands, with the model protein bovine pancreatic ribonuclease (RNase A) by means of UV–visible absorption spectroscopy, circular dichroism (CD), electrospray ionization mass spectrometry (ESI-MS) and X-ray crystallography. It is the first attempt to investigate the binding of a neutral diruthenium compound to a protein. ESI-MS data indicate that, in solution, under the investigated experimental conditions, the diruthenium compound binds the protein upon the loss of an acetate ligand. The crystallographic results indicate the replacement of an acetate by two water molecules and the coordination of the $[Ru_2(D\text{-}p\text{-}FPhF)(O_2CCH_3)_2(O_2CO)(OH_2)_2]^+$ ion, that is expected to be a highly reactive species in the absence of the protein, to the imidazole ring of His105 at the axial site. The side chains of Glu9 and His119 are also identified as possible diruthenium binding sites. The binding significantly affects the protein ability to form dimers and higher-order oligomers, without significantly altering its secondary structure content and thermal stability. These data show that: i) Glu side chain has to be considered as a possible alternative binding site for diruthenium compounds, ii) diruthenium containing fragments that would be unstable in solution can be formed upon reaction of diruthenium compounds with a protein, iii) diruthenium compounds could be used as modulators of protein aggregation.

1. Introduction

Metallodrugs have become important competitors of purely organic agents thanks to their structural and physicochemical properties, comprising structural variety, accessible redox states, a wide spectrum of coordination numbers and geometries, and the possibility to fine-tune ligand substitution thermodynamics and kinetics [1–6]. In this respect, paddlewheel Ru_2^{5+} complexes have been used as molecular building blocks to develop new metallodrugs with anticancer properties [5,7–17]. The biological activity of these species has been increased by coordinating biologically active carboxylate ligands (drugs) to the bimetallic core. The comparison between the biological activities of the free drugs and of the drugs bound to the diruthenium center demonstrates that the coordination to the inorganic core improves drug activity. The bimetallic unit is not just a mere drug carrier; indeed, there is a synergistic effect between the drug and the diruthenium core [13,15,17]. Besides its antitumor action, other biological properties have been described for diruthenium species, such as pH-responsive delivery systems [18,19], RNA probing compounds [20], or inhibitors of amyloid-β aggregation [21,22].

The most common type of diruthenium compounds contains four carboxylate bridging (RCO_2^-, R = aryl, allyl, or alkyl) ligands in equatorial positions arranged in a lantern-like fashion and σ and/or π-donating electron rich ligands at the axial positions [23]. However, this is not the sole possibility. Different research groups have used the $[Ru_2Cl(O_2CCH_3)_4]$ compound as starting material to synthesize new derivatives based on the partial substitution of acetate ligands (mono-, di- or tri-substituted species) by *N,N*-donor (*e.g.* amidinates or

☆ This article is dedicated to Dr. Ana Edilia Sánchez Peláez on her retirement. Thank you for your great vocation as a professor and researcher.

* Corresponding author.
E-mail address: antonello.merlino@unina.it (A. Merlino).

https://doi.org/10.1016/j.ijbiomac.2024.137691
Received 4 October 2024; Received in revised form 11 November 2024; Accepted 13 November 2024
Available online 17 November 2024

aminopyridinates), *N*,*O*-donor (*e.g.* amidates) bridging ligands or even monodentate or low coordinating ligands [24–32]. The precise control of the synthetic conditions (temperature, solvent, atmosphere, or reagents ratio) is essential to obtain these derivatives. The properties of these intermediate species differ significantly from the tetrasubstituted diruthenium compounds in terms of solubility, geometry, electrochemical properties, and reactivity.

The interaction of different mono- and di-substituted diruthenium compounds with the model proteins Hen Egg White Lysozyme (HEWL) and bovine pancreatic ribonuclease (RNase A) has been recently characterized [33–35]. These studies were carried out to understand the mechanism of action of diruthenium metallodrugs. The results suggest that biological macromolecules could play a major role in the delivery and targeting of these compounds. Literature data report the interaction of diruthenium paddlewheel complexes with nucleic acids [20] and proteins both from the experimental [36] and computational points of view [37,38]. For example, the open-paddlewheel diruthenium compound $[Ru_2Cl_2(DPhF)_3(DMSO)]$ ($DPhF^- = N,N'$-diphenylformamidinate and DMSO = dimethylsulfoxide) can bind RNA at positions located one or two nucleotides away from junctions or bulges of the nucleic acid structure [20] and the $[Ru_2Cl(O_2CCH_3)_4]$ compound can bind HEWL at the Asp side chains replacing the acetate ligands [36]. Our groups have demonstrated that the protein binding properties of diruthenium compounds depend on charge and steric hindrance, as postulated by theoretical calculations [37,38]. The complexes $[Ru_2(L\text{-}L)(O_2CCH_3)_3]^+$ (where L-L = $DPhF^-$; D-*p*-$FPhF^-$ = *N*,*N*′-*bis*(4-fluorophenyl)formamidinate; or $DAniF^-$ = *N*,*N*′-*bis*(4-methoxyphenyl)formamidinate) and $[Ru_2(DPhF)_2(O_2CCH_3)_2]^+$ can interact with HEWL through the Asp side chains, but also can bind Lys and Arg side chains or even main chain carbonyl groups at the axial site [33]. When the same protein is treated with the compounds $[Ru_2(L\text{-}L)(CO_3)_3]^{2-}$, non-covalent binding of the diruthenium compound is observed [34]. The difference in protein binding capacity between these two families of diruthenium compounds arises from the charge of the complexes in solution: negatively charged complexes bind the protein non-covalently, while cationic complexes bind the protein by coordination of the Ru_2 centre to protein atoms. It is worth mentioning that anionic diruthenium complexes can replace their ligands in solution, changing their charge and favouring the covalent binding [35].

Recently, we have described the first artificial diruthenium metalloprotein resulting upon reaction of $[Ru_2Cl(D\text{-}p\text{-}CNPhF)(O_2CCH_3)_3]$ (D-*p*-$CNPhF^-$ = *N*,*N*′-*bis*(4-cyanophenyl)formamidinate) with the model protein bovine pancreatic ribonuclease (RNase A), which has been frequently used to study metalation processes [39–41]. In this case, the $[Ru_2(D\text{-}p\text{-}CNPhF)(O_2CCH_3)_2(OH_2)_2]^+$ fragment binds through one axial position the side chain of His105, which is located on the protein surface. The crystallographic results in combination with first principles calculations have revealed the important role played by the protein environment in the protein binding and ligand exchange around the Ru_2 core [42]. Diruthenium compounds have been also used as inhibitors of amyloid peptide aggregation. In particular, it has been shown that $[Ru_2Cl(DPhF)(O_2CCH_3)_3]\cdot H_2O$, $[Ru_2Cl(DPhF)_2(O_2CCH_3)_2]\cdot H_2O$, $[Ru_2Cl(D\text{-}p\text{-}FPhF)(O_2CCH_3)_3]\cdot H_2O$ and $K_3[Ru_2(CO_3)_4]\cdot 3H_2O$ act as inhibitors of the $A\beta_{1-42}$ peptide aggregation. $K_2[Ru_2(DPhF)(CO_3)_3]\cdot 3H_2O$ and $[Ru_2Cl(D\text{-}p\text{-}FPhF)(O_2CCH_3)_3]\cdot H_2O$ also inhibit aggregation of $A\beta_{1-42}$ peptide fragments $A\beta_{1-16}$ and $A\beta_{21-40}$ [21,22].

The wide knowledge achieved on the interaction of charged diruthenium compounds with proteins has no counterpart when it comes to neutral diruthenium species in solution, whose reactivity is largely unexplored. The aim of this work is to study the protein binding properties of a new neutral diruthenium compound, $[Ru_2(D\text{-}p\text{-}FPhF)(O_2CCH_3)_2(O_2CO)]\cdot 3H_2O$ (Fig. 1), here synthetized for the first time. This complex is not only a neutral compound, but also a very rare example of a diruthenium compound with three different equatorial ligands reported to date. We have studied the properties of this new compound, as well as its interaction with the model protein RNase A using a combined spectroscopic/spectrometric/crystallographic approach. The ability of the compound to act as modulator of the protein aggregation process has been also evaluated, together with its ability to alter protein thermal stability.

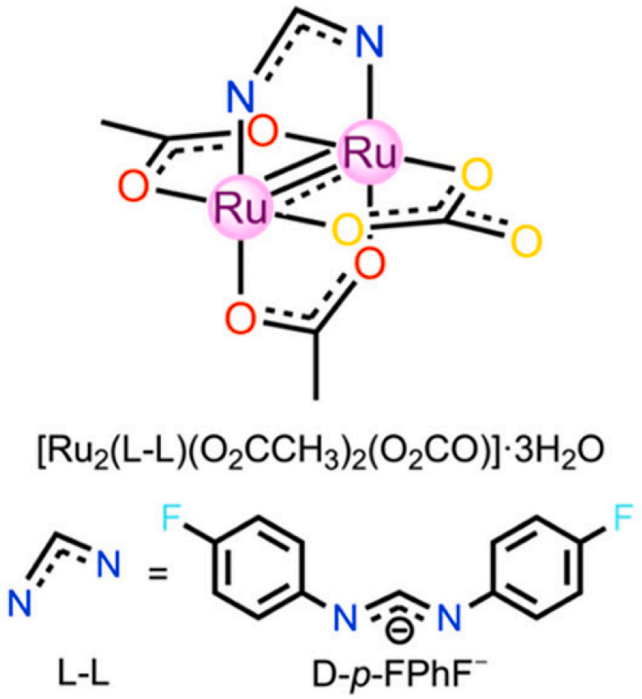

Fig. 1. Core structure of the $[Ru_2(D\text{-}p\text{-}FPhF)(O_2CCH_3)_2(O_2CO)]\cdot 3H_2O$ complex. Water molecules are omitted for the sake of clarity.

2. Experimental

2.1. Synthesis of $[Ru_2(D\text{-}p\text{-}FPhF)(O_2CCH_3)_2(O_2CO)]\cdot 3H_2O$.

All the reactions and manipulations were performed under air atmosphere. All reactants and solvents were obtained from commercial sources and used without further purification unless otherwise indicated. The HD-*p*-FPhF formamidine was prepared according to a published general procedure [43]. The diruthenium starting materials, $[Ru_2Cl(O_2CCH_3)_4]$ and $[Ru_2Cl(D\text{-}p\text{-}FPhF)(O_2CCH_3)_3]\cdot H_2O$, were previously reported [24,44].

To a red solution of $[Ru_2Cl(D\text{-}p\text{-}FPhF)(O_2CCH_3)_3]\cdot H_2O$ compound (0.066 g, 0.1 mmol) in ethanol (Sigma-Aldrich, purity ≥95 %, 20 mL) was added a colorless solution of K_2CO_3 (Sigma-Aldrich, purity ≥99 %, 0.011 g, 0.1 mmol) in distilled water (0.3 mL) at room temperature. After stirring for 5 h, it was added 1 mL of a solution of $AgNO_3$ (Sigma-Aldrich, purity ≥ 99 %, 0.1 M) (Scheme 1). The resultant red-orange suspension was stirred for 24 h with the strict exclusion of light. The reaction mixture was then filtered through Celite® to remove AgCl, and

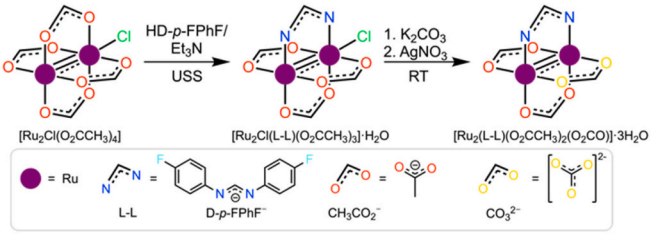

Scheme 1. Reaction pathway to prepare $[Ru_2(D\text{-}p\text{-}FPhF)(O_2CCH_3)_2(O_2CO)]\cdot 3H_2O$. Water molecules have been omitted for the sake of clarity.

the solvent was dried *in vacuo* to give a dark orange powder. The solid was solved in distilled water (150 mL), and the solution was placed in a separatory funnel to be extracted first with CH_2Cl_2 (Sigma-Aldrich, purity ≥ 99 %, 50 mL) to remove $[Ru_2Cl(D\text{-}p\text{-}FPhF)(O_2CCH_3)_3]\cdot H_2O$ compound, and then with EtOAc (Sigma-Aldrich, purity ≥ 99 %, 5×100 mL). To the EtOAc solution, $MgSO_4$ (Sigma-Aldrich, purity ≥ 99 %) was added, then filtered off, and concentrated to dryness. The product was dried under vacuum. Yield: 0.028 g, 42 %. Anal. Calcd for $C_{18}H_{21}F_2N_2O_{10}Ru_2$ (665.51 g/mol): C, 32.49; H, 3.18; N, 4.21 %. Found: C, 32.38; H, 3.27; N, 4.07 %. ESI (*m/z*): 611.6 $[M - 3H_2O]^+$.

2.2. Characterization of $[Ru_2(D\text{-}p\text{-}FPhF)(O_2CCH_3)_2(O_2CO)]\cdot 3H_2O$

ATR-FTIR spectrum (4000–500 cm^{-1}) was recorded with a Perkin-Elmer Spectrum 100 with a universal ATR accessory. Elemental analysis was performed at the Microanalytical Service of the Complutense University of Madrid. Mass spectrometry data (electrospray ionization) were recorded at the Mass Spectrometry Service of the Complutense University of Madrid, using an ion trap analyzer HCT Ultra (Bruker Daltonics) mass spectrometer in water solution.

2.3. Computational details

All calculations were performed using the Gaussian 16 program suite [45]. The structural optimization of the diruthenium isomeric complexes was computed at the DFT-B3LYP level of theory [46]. Geometries were fully optimized with no symmetry constrains. The Def2TZVP basis set was used for C, H, N, O, and F atoms while the SDD effective core potential and basis set were used for Ru atoms. Water was considered within the Solvent Model Density (SMD) implicit solvation approach [47]. Frequency calculations were performed on all optimized geometries to ensure that the obtained structures represent local minima.

2.4. Protein binding studies

2.4.1. UV–visible absorption spectroscopy

RNase A (Sigma-Aldrich, type XII A; purity ≥ 90 %, SDS-PAGE) was used without further purification. The stability of $[Ru_2(D\text{-}p\text{-}FPhF)(O_2CCH_3)_2(O_2CO)]\cdot 3H_2O$ was studied by UV–visible spectroscopy in the experimental condition used to grow RNase A crystals, *i.e.* 22 % PEG4K (Sigma-Aldrich, purity 100 %), and 10 mM sodium citrate buffer (Sigma-Aldrich, purity > 99.5 %) at pH 5.0, and in the buffer used to collect ESI-MS spectra, *i.e.* 10 mM ammonium acetate (Sigma-Aldrich, purity > 99.0 %) buffer pH 6.8.

UV–visible absorption spectra were recorded at 25 °C using a 1.0 cm pathlength quartz cells on a JASCO V-750 UV–visible spectrophotometer in the range of 200–700 nm, using a diruthenium compound concentration of 50 μM in milliQ water. Other experimental parameters were: bandwidth 2.0 nm, scanning speed 200 nm/min, data pitch 1.0 nm. UV–visible spectra were collected in the absence and in the presence of RNase A. The RNase A:Ru_2 molar ratio was 1:3. Each measurement was repeated three times.

2.4.2. Circular dichroism spectroscopy

Far UV-CD spectra were recorded on a Jasco J-1500 spectropolarimeter equipped with a Peltier thermostatic cell holder using a 0.1 cm path length quartz cell. Spectra were registered at 25 °C in the range of 195–250 nm at a protein concentration of 7.3 μM in 10 mM sodium citrate buffer at pH 5.0 and 10 mM ammonium acetate buffer at pH 6.8. Measurements were recorded with a time constant of 2 s, 2 nm bandwidth, and scan rate of 50 nm/min. Three scans for each spectrum were acquired.

2.5. Crystallization of the adduct formed upon reaction of $[Ru_2(D\text{-}p\text{-}FPhF)(O_2CCH_3)_2(O_2CO)]\cdot 3H_2O$ with RNase A

Metal-free RNase A crystals were grown by hanging drop vapor diffusion using RNase A at 20 $mg\cdot mL^{-1}$ concentration and a reservoir solution containing 22 % PEG4K and 10 mM sodium citrate buffer at pH 5.0. Crystals grew in two weeks and were soaked in a reservoir solution saturated with $[Ru_2(D\text{-}p\text{-}FPhF)(O_2CCH_3)_2(O_2CO)]\cdot 3H_2O$ for three days.

2.6. Data collection and refinement

X-ray diffraction data were collected at XRD2 beamline of Elettra synchrotron of Trieste, Italy. Crystals were flash-frozen at 100 K using liquid nitrogen (and maintained at 100 K during the data collection). X-ray diffraction data were processed using Autoproc [48]. The structure was solved by molecular replacement using the program Phaser of CCP4i suite [49] and model derived from PDB code 1JVT (molecule A) [50]. The building of the model was carried out using Coot [51]. The structure was refined using REFMAC5 [52]. Data collection and refinement statistics are summarized in Table S1. Coordinates and structure factors were deposited in the Protein Data Bank under the accession code 9GYS.

2.7. ESI-MS experiments

Sample preparation: a stock solution of RNase A (Sigma-Aldrich, type XII A; purity ≥ 90 %, SDS-PAGE) 10^{-3} M was prepared dissolving the lyophilized protein in LC-MS grade water. A stock solution of the diruthenium compound was prepared by dissolving the samples in water to a final concentration of 10^{-2} M. For the measurements, an aliquot of the stock solution of the protein was mixed with an aliquot of the diruthenium compound at protein-to-metal ratio of 1:3 and then diluted with LC-MS grade water to a final protein concentration of 100 μM. The mixture was incubated at a temperature of 37 °C up to 10 days. Instrumental measurements were conducted at intervals of 24, 48, and 72 h. After the incubation time, the protein solution was sampled and diluted to a final protein concentration of 500 nM using LC-MS grade water by adding 0.1 % *v/v* of formic acid just before the infusion in the mass spectrometer.

Instrumental parameters: the ESI mass spectra were acquired through direct infusion at 7 $\mu L\cdot min^{-1}$ flow rate in a Tri-pleTOF® 5600+ high-resolution mass spectrometer (Sciex, Framingham, MA, U.S.A.), equipped with a DuoSpray® interface operating with an ESI probe.

The ESI source parameters were as follows:

RNase A: positive polarity, Ionspray Voltage Floating 5500 V, Temperature 0, Ion source Gas 1 (GS1) 40 L/min; Ion source Gas 2 (GS2) 0; Curtain Gas (CUR) 15 L/min, Declustering Potential (DP) 100 V, Collision Energy (CE) 10 V, acquisition range 1000–2600 *m/z*.

For acquisition, Analyst TF software 1.7.1 (Sciex) was used, and deconvoluted spectra were obtained by using the Bio Tool Kit micro-application v.2.2 embedded in Peak-ViewTM software v.2.2 (Sciex).

2.8. Aggregation studies

3.0 mg of RNase A were dissolved in 300 μL of 40 % acetic acid for the lyophilization. The lyophilized protein was then suspended in 300 μL of 0.2 sodium phosphate buffer at pH 6.7 and incubated at 37 °C for 2 h, in the presence and in the absence of the metal compound. Finally, 100 μL of this solution were loaded on a gel-filtration column.

Gel filtration chromatography was performed on a Superdex 75 10/300 GL column attached to an ÄKTA prime plus fast protein liquid chromatography (FPLC) system, equilibrated and eluted with 0.4 M sodium phosphate pH 6.7, at a flow rate of 0.10 $mL\cdot min^{-1}$, according to the procedure described in reference [53].

3. Results and discussion

3.1. Design of $[Ru_2(D\text{-}p\text{-}FPhF)(O_2CCH_3)_2(O_2CO)]\cdot 3H_2O$

$[Ru_2Cl(O_2CCH_3)_4]$ is the most common starting material in the synthesis of diruthenium compounds. This species enables diverse ligand exchange possibilities, from partial (mono-, di-, or tri-substituted species) to total replacement of the acetate ligands, with their properties being tunable by the nature of the ligand, the substitution degree and the particular ligand configurations [31,54]. Within the family of partial substitution compounds, generally only two different ligands are present at the equatorial positions. Up to very recently, there are some examples with two different bridging ligands [55–57], but examples in literature of diruthenium complexes with three or four different equatorial ligands coordinated to the bimetallic core are very rare [32].

Here, we synthetize a diruthenium complex with a neutral charge and three different equatorial ligands: two acetates, one carbonate and one formamidinate. To achieve this goal, we reacted the $[Ru_2Cl(D\text{-}p\text{-}FPhF)(O_2CCH_3)_3]\cdot H_2O$ complex with an equimolar amount of K_2CO_3, so that one acetate could be replaced by one carbonate ligand. Then, an excess of $AgNO_3$ was added to remove the axial chloride ligand. The substitution reaction of acetate ligand by carbonate ligand proceeds rapidly under mild conditions and, after 5 h, the starting product had been practically converted. The new complex is air-stable, water-soluble, and can be handled without special caution.

The features of the new complex were determined by elemental analysis, ATR-FTIR (attenuated total reflection Fourier transform infrared) spectroscopy, UV–visible absorption spectroscopy, Electrospray ionization mass spectrometry (ESI-MS), and Density Functional Theory (DFT) calculations.

The elemental analysis for the bulk powder sample is in good agreement with the calculated values for a complex with the formula $[Ru_2(D\text{-}p\text{-}FPhF)(O_2CCH_3)(O_2CO)]\cdot 3H_2O$. The vibrational spectrum of this complex was recorded in the range 4000–500 cm^{-1} (Fig. S1, ESI) and is very similar to that of the analogue compound with three acetate ligands [31]. We observed a wide band in the range 3500–3200 cm^{-1} and a band centred around 1640 cm^{-1}, which suggest the presence of water in the complex, in accordance with elemental analysis. The removal of the axial chloride ligand leaves free both axial positions of the Ru_2 core. Therefore, it is expected that they may be occupied by water molecules, as in other mono- and bi-substituted diruthenium derivatives [24,30,31,58]. The vibrational modes of acetates/carbonate ligands are very close. We can observe them at 1528 cm^{-1} (asymmetric COO stretching), 1436 cm^{-1} (symmetric COO stretching), and 687 cm^{-1} (COO bending). The difference between the symmetric and asymmetric COO frequencies ($\Delta\nu = \nu_a - \nu_s$) is evidence of the coordination type. In this case, the separation of the wave numbers (92 cm^{-1}) suggests a bidentate-type coordination [59]. Finally, the formamidinate ligand shows vibrational modes at 1494, 1310, and 1202 cm^{-1}, corresponding to CN and CC aromatic stretches, and CH bending, respectively (Fig. S1, ESI). These results confirmed the presence of representative functional groups coordinated to the diruthenium core.

ESI-MS was used to verify the stoichiometry and elemental composition of the diruthenium complex. The mass spectrum supports the exchange of only one acetate ligand by one carbonate ligand, and the retention of the formamidinate ligand (Fig. S2, ESI). The dominant peak corresponds to the intact complex with the loss of water molecules, $[M - 3\cdot H_2O]^+$.

Such experimental characterization does not permit to determine the substitution position of the $[RuCl(D\text{-}p\text{-}FPhF)(O_2CCH_3)_3]\cdot H_2O$ species, since the complex shows three different feasible coordination positions for the carbonate ligand: two *cis* and one *trans* with respect to the formamidinate ligand. Attempts to obtain suitable single crystals for X-ray diffraction studies failed. To clarify this aspect, we relied on first-principles calculations [60]. DFT was used to optimize the ground-state structures of both possible isomers, *cis*-$[Ru_2(D\text{-}p\text{-}FPhF)(O_2CCH_3)_2(O_2CO)]$ and *trans*-$[Ru_2(D\text{-}p\text{-}FPhF)(O_2CCH_3)_2(O_2CO)]$. The optimized geometrical parameters, collected in Figs. S3 and S4 (ESI), deliver computed bond lengths in good agreement with those obtained for other partially substituted Ru_2^{5+} compounds.

Energetically speaking, we reported recently for a similar complex that the most favored substitution position was in the *cis* position with respect to the formamidinate ligand, which switched to the *trans* position under high steric hindrance conditions [42]. Here, quantum mechanical calculations show that the *cis*-isomer (Fig. 1) is 1.8 kcal/mol more stable than the *trans*-isomer. This is expected since the carbonate ligand is not a bulky ligand that can cause steric clashes around the diruthenium core. The different stability of the isomers can be ascribed to orbital overlap-related electronic effects. Indeed, the *trans* compound shows a weaker σ bond between the Ru_2 core and the formamidinate ligand, which results in longer Ru—N distances. This appears to be associated with a slight destabilization of the HOMO, which involves the $Ru_2(\delta^*)$ orbital and the pπ lone pairs of the formamidinate ligand (Fig. 2). These results permit to explain why the vast majority of bi-substituted paddlewheel complexes show a *cis* configuration [54,58].

3.2. Reactivity with RNase A: in solution studies

The reactivity of $[Ru_2(D\text{-}p\text{-}FPhF)(O_2CCH_3)_2(O_2CO)]\cdot 3H_2O$ with RNase A has been first studied in solution by UV–visible absorption spectroscopy, circular dichroism and ESI-MS.

3.3. UV–visible absorption spectroscopy and circular dichroism

UV–visible absorption spectra of $[Ru_2(D\text{-}p\text{-}FPhF)(O_2CCH_3)_2(O_2CO)]\cdot 3H_2O$ were recorded under two conditions in the absence (Fig. 3A and C) and presence of RNase A (Fig. 3B and D) overtime (up to seven days). These experimental conditions were chosen because they were used to crystallize RNase A and to study the reactivity of metal compounds with the protein *via* ESI-MS [61]. Under both experimental conditions, spectra of the compound showed bands around 227 nm and 345 nm and one band of low intensity around 510 nm. The UV band at 227 nm can be assigned to an axial ligand-to-metal charge transfer, while the lowest energy band could be assigned to a mixture of transitions: π(Ru-N/O, Ru_2) → δ*(Ru_2), σ(Ru_2/axial) → π*(Ru_2), π*(Ru_2) → σ*(Ru_2/axial) and π(Ru_2) → π*(N/O)/δ*(Ru_2) [62]. Following previous assignments, [58] the band at 345 nm could be attributed to ligand-to-metal transitions [π(N) → σ*/π*/δ*(Ru_2)]. The spectral profiles of $[Ru_2(D\text{-}p\text{-}FPhF)(O_2CCH_3)_2(O_2CO)]\cdot 3H_2O$ do not experience significant variations over seven days under both the investigated experimental conditions. Similar results were obtained in the presence of the protein (Fig. 3B and D).

CD spectra of RNase A in the presence of $[Ru_2(D\text{-}p\text{-}FPhF)(O_2CCH_3)_2(O_2CO)]\cdot 3H_2O$ in 10 mM sodium citrate buffer pH 5.0 (Fig. 4A) and in 10 mM ammonium acetate pH 6.8 (Fig. 4B) were recorded to evaluate the effect of the metal compound binding on the secondary structure of the protein. CD measurements suggest that the protein retains its secondary structure in the presence of the metal compound, although a slight variation of molar ellipticity is observed when the protein to metal molar ratio is changed. CD has been also used to evaluate the thermal stability of the adduct and to compare its melting temperature with that of the metal-free protein. The CD melting temperatures (T_m) for the metal-free RNase A and for the protein in the presence of the diruthenium complex in 1:3 protein to metal ratio are 66 ±1 and 65±1 °C, respectively, in 10 mM sodium citrate at pH 5.0, and 61±1 and 62±1 °C, respectively, in 10 mM ammonium acetate at pH 6.8. The T_m values of the metal-free protein agree with that found in our laboratory in the past (65±1 °C in 10 mM sodium citrate at pH 5.0) [53]. Similar results have been obtained using a phosphate-free protein sample, obtained upon removing the residual phosphate ion present in the protein active site, after treating the protein at pH 9.0. These findings suggest that the Ru_2 compound does not alter the RNase A thermal stability.

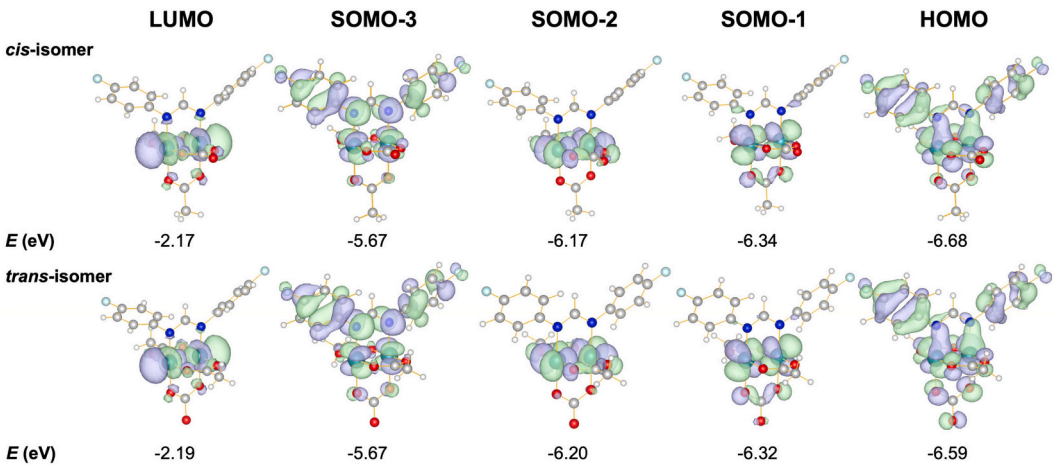

Fig. 2. Frontier molecular orbitals of the *cis*- and *trans*-isomers obtained by DFT-B3LYP calculations (isosurface-value = 0.03) and corresponding energies. Atoms colour code: white H, grey C, dark blue N, red O, light blue F, and teal Ru.

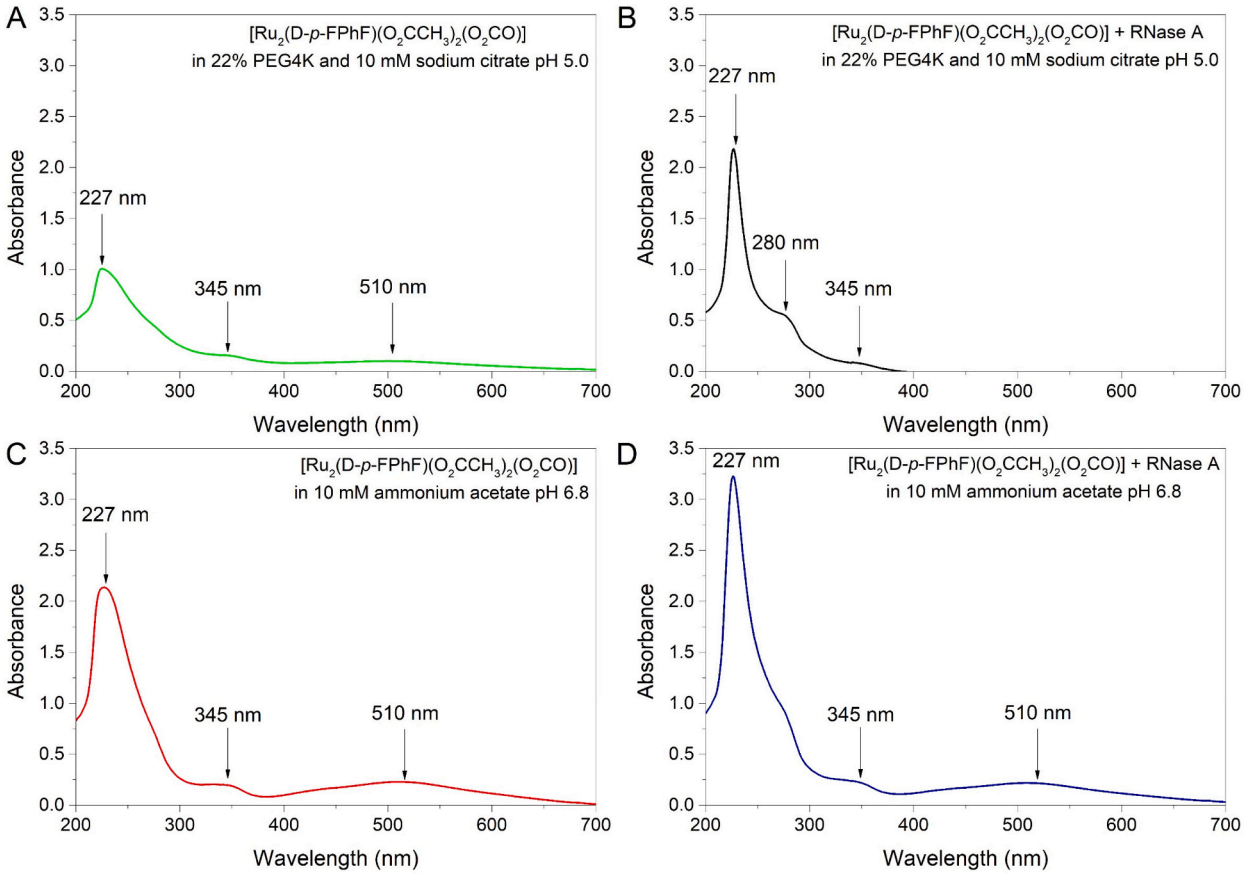

Fig. 3. Time course UV–vis absorption spectra of $[Ru_2(D\text{-}p\text{-}FPhF)(O_2CCH_3)_2(O_2CO)]$ (50 μM) in 22 % PEG4K and 10 mM sodium citrate at pH 5.0 (A) and in 10 mM ammonium acetate at pH 6.8 (C). Spectra under the same conditions but in the presence of RNase A are reported in panels B and D (molar ratio 1:3 RNase A/Ru_2). The wavelengths of each peak on the spectra are also reported. No appreciable spectral changes were observed within 7 days.

3.4. Electrospray ionization mass spectrometry

A series of protein binding studies were then performed using an ESI-MS experimental protocol developed by the METMED laboratory in Florence [63,64]. This protocol enabled the characterization of protein metalation by Pt [61], V [65], Au [66], Rh [67], Ir [68] compounds. Specifically, RNase A was reacted with $[Ru_2(D\text{-}p\text{-}FPhF)(O_2CCH_3)_2(O_2CO)]\cdot 3H_2O$ and the resulting products were analyzed *via* ESI-MS.

Fig. 5 displays the ESI mass spectrum of RNase A after 24 h of incubation with $[Ru_2(D\text{-}p\text{-}FPhF)(O_2CCH_3)_2(O_2CO)]$ at 37 °C. Additional spectra at different incubation times and metal-to-protein ratios are provided in the Supporting Information (Fig. S5, ESI). Spectral analysis indicates that the species resulting from the loss of an acetate ligand, *i.e.* $([Ru_2(D\text{-}p\text{-}FPhF)(O_2CCH_3)(O_2CO)]^+)$, forms adducts with RNase A. These adducts can contain one or two metallic fragments, with masses of

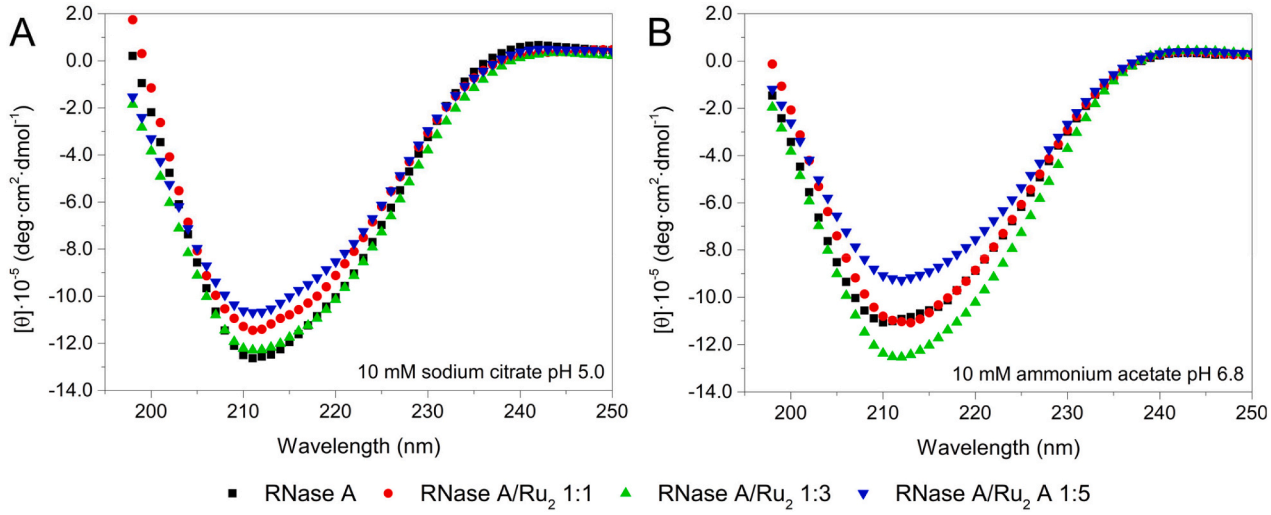

Fig. 4. CD Spectra of RNase A (7.3 μM) in the absence (black) and in the presence of $[Ru_2(D\text{-}p\text{-}FPhF)(O_2CCH_3)_2(O_2CO)]\cdot 3H_2O$ in different protein to metal molar ratios in 10 mM sodium citrate pH 5.0 (panel A) and in 10 mM ammonium acetate pH 6.8 (panel B).

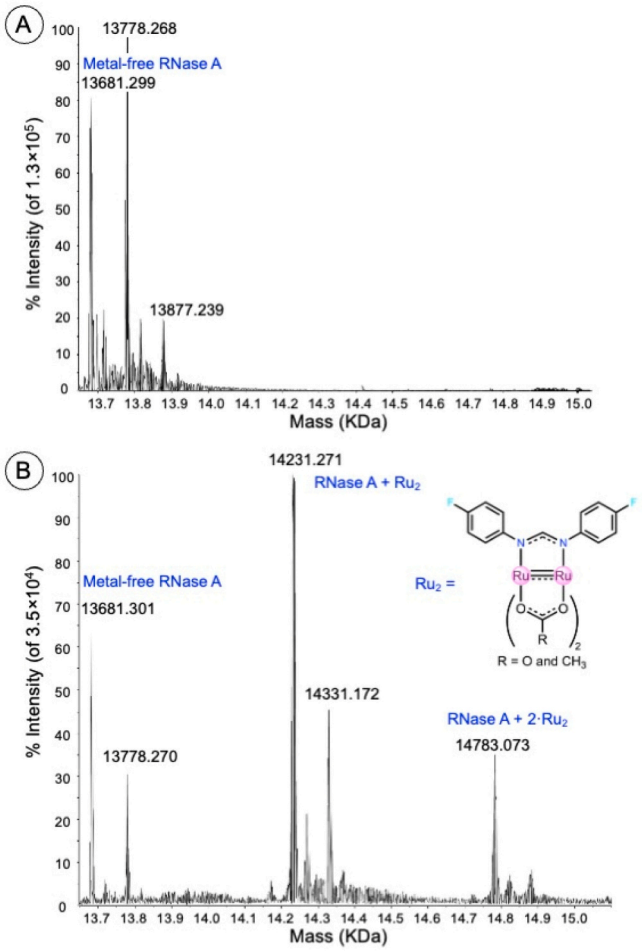

Fig. 5. Deconvoluted ESI-MS of A) metal-free RNase A (5×10^{-7} mol·L^{-1}) and of B) RNase A treated with $[Ru_2(D\text{-}p\text{-}FPhF)(O_2CCH_3)_2(O_2CO)]$ in a protein: metal ratio = 1:3 in LC-MS grade water and recorded after 24 h of incubation at 37 °C.

14,231 Da and 14,782 Da, respectively.

In addition to these adducts, we also observed a signal at 13,681 Da, ascribable to the non-metalated protein. Moreover, two more peaks at 13,779 Da and 13,877 Da, likely resulting from interactions between the protein and salt ions (such as phosphate or sulphate) present in the commercial protein sample, were detected. Indeed, these peaks were already observed in the ESI-MS spectra of the metal-free protein in other works [67].

3.5. Reactivity with RNase A: structural studies

The reaction of $[Ru_2(D\text{-}p\text{-}FPhF)(O_2CCH_3)_2(O_2CO)]\cdot 3H_2O$ with RNase A has been also studied in the solid state by means of X-ray crystallography. Native RNase A crystals were soaked in a reservoir solution saturated with the Ru_2 compound powder for three days and tested by X-ray diffraction. They contain two protein molecules (hereafter denoted as molecule A and molecule B) in the asymmetric unit (a.u.). Data collection and refinement statistics are reported in Table S1. Root mean square deviation of Cα atoms (rmsd) between the two molecules is 0.427 Å, while 0.254 Å is the average rmsd value from the structure of the metal-free protein (PDB code 1JVT) [50].

The overall structure of the adduct formed upon reaction of RNase A with $[Ru_2(D\text{-}p\text{-}FPhF)(O_2CCH_3)_2(O_2CO)]\cdot 3H_2O$ is reported in Fig. 6. The adduct was refined at high resolution (1.74 Å). In molecule A, three diruthenium motifs were observed at level of the side chain of His105 (occupancy = 0.45), His119 (occupancy = 0.50), and Glu9 (occupancy = 0.45) (Fig. 7A-C). In molecule B, two diruthenium containing fragments bound to the side chain of His105 (occupancy = 0.45) and His119 (occupancy = 0.50) (Fig. 7D and E) were found. His119 is a catalytically important residue located in the protein active site [69], while His105 is on the protein surface. The side chain of Glu9 is hydrogen bonded to water molecules in molecule B (Fig. S6, ESI). This residue is located on the N-terminal helix.

His105 has been previously identified as a binding site for diruthenium [42] and dirhodium [67,70] compounds, while His119 has just been involved in the recognition of mono- and bi-nuclear compounds containing Pt [53,71,72], Ru [73–75], Rh [67], Pd [76], Ir [68], As—Pt [77] and Au [66] based-drugs. The side chain of Glu9 has never been identified as a potential metal-binding site.

Although electron density maps for the ligands in all the Ru_2 binding sites are not well defined, metal ligands can be confidently modelled close to the side chain of His105 in molecule B. In particular, at this site, a $[Ru_2(D\text{-}p\text{-}FPhF)(O_2CCH_3)(O_2CO)(OH_2)_2]^+$ fragment was found axially coordinated to His105 side chain (Fig. 7D). A superposition of this binding site with that observed for the $[Ru_2(D\text{-}p\text{-}CNPhF)(O_2CCH_3)_2(OH_2)_2]^+$ fragment indicates a strict similarity in the

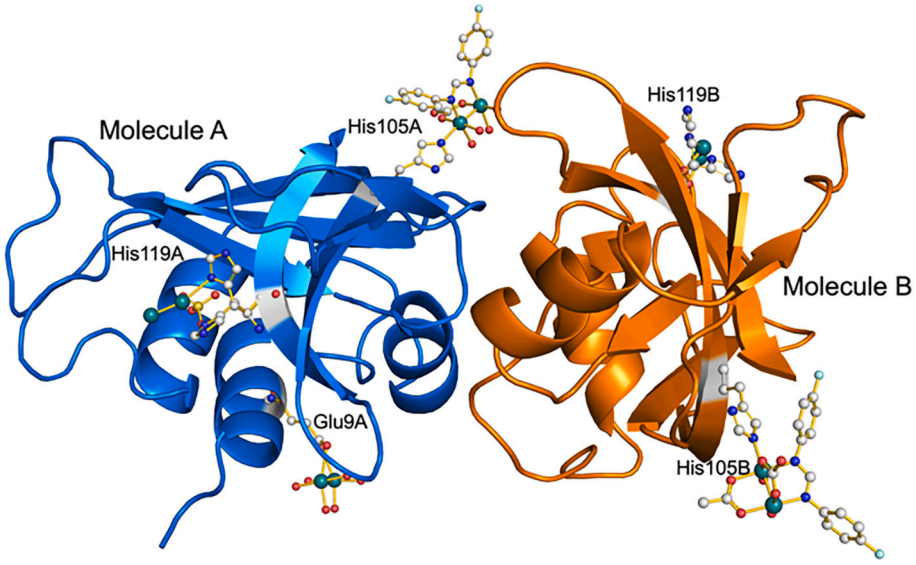

Fig. 6. Overall structure of the two RNase A molecules (A in blue and B in orange) in the asymmetric unit of the crystal of the adduct formed upon reaction of $[Ru_2(D\text{-}p\text{-}FPhF)(O_2CCH_3)_2(O_2CO)]\cdot 3H_2O$ with RNase A at the solid state. Ru2 binding sites are also shown and evidenced in grey. (For interpretation of the references to colour in this figure legend, the reader is referred to the web version of this article.)

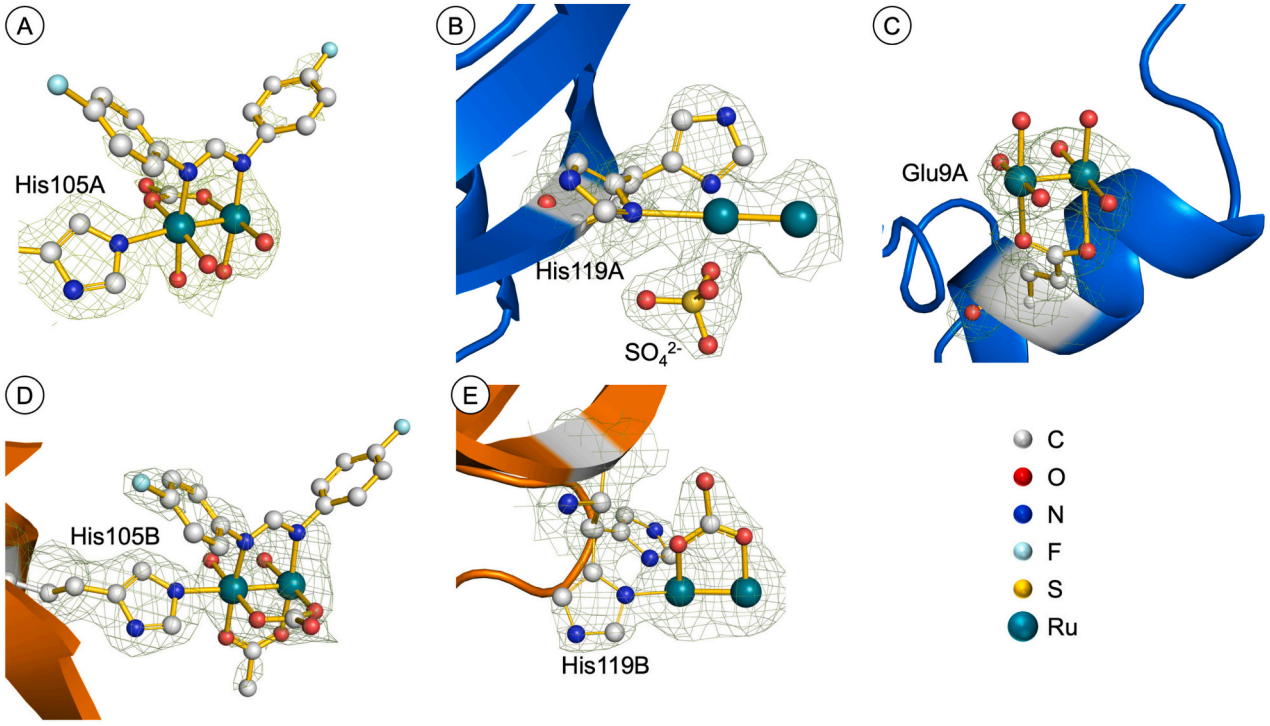

Fig. 7. Details of diruthenium binding sites in the adduct formed upon reaction of $[Ru_2(D\text{-}p\text{-}FPhF)(O_2CCH_3)_2(O_2CO)]\cdot 3H_2O$ with RNase A at the solid state: His105 (panel A), His119 (panel B) and Glu9 (panel C) of molecule A, His105 (panel D) and His119 (panel E) of molecule B. 2Fo-Fc electron density maps are contoured at 1σ level (in light green).

recognition of the two diruthenium moieties by the protein (Fig. S7). The loss of an acetate ligand in the structure here reported agrees with mass spectrometry data, while its replacement by water molecules is in agreement with our previous observation that the binding of a His residue at the axial position favours the replacement of equatorial acetate ligands by water molecules [42], stabilizing metal containing fragments that would be highly reactive in the absence of the protein. The carbonate group of this fragment is *cis* with respect to D-*p*-$FPhF^-$, in agreement with what predicted by quantum chemical calculations. The presence of the CO_3^{2-} ligand is confirmed by the formation of hydrogen bonds between the free oxygen (*i.e.* the oxygen not coordinated to the diruthenium centre) and water molecules that in turns are bound to atoms of Tyr76 and Gln64. The binding of the $[Ru_2(D\text{-}p\text{-}FPhF)(O_2CCH_3)(O_2CO)(OH_2)_2]^+$ fragment to the protein is further stabilized by the hydrogen bond that one of the two molecules that replace the acetate ligand forms with a water molecule that in turn is in contact with the C-terminal tail.

In molecule A, close to the same His side chain, the electron density

map is less clearly defined. However, a $[Ru_2(D\text{-}p\text{-}FPhF)(O_2CO)(OH_2)_4]^{2+}$ ion has been tentatively modelled (Fig. 7A). Here, the presence of the CO_3^{2-} ligand is confirmed by the formation of hydrogen bonds between the free oxygen and water molecules that are in turn bound to atoms of Asn103 and to the C-terminal carboxylate. However, we cannot exclude that actually two water molecules can be a disordered acetate, as in molecule B. Anyway, comparing the position of the carbonate ligands in the metal containing fragments bound to the His105A and His105B side chains (Fig. 7A and D), it appears clear that the metal complex adopts a different conformation in the two protein molecules in the asymmetric unit.

The metal containing moieties that are bound to the protein are even more difficult to be assigned in the protein active sites, where the interpretation of the e.d. maps is ulteriorly complicated by the presence of a residual amount of sulphate/phosphate and of alternative conformations of His119 (Fig. 7B and E). The existence of alternative conformations of catalytically important His119 is well known [78]. Our findings demonstrate that the presence of the diruthenium center does not affect the flexibility of this residue. The best interpretation of the e.d. maps at these sites suggests the presence of bimetallic fragments which could adopt alternative conformations. The unclear electron density maps allowed the modelling of a sulphate/phosphate ion alternative to the metallic fragment in molecule A (Fig. 7B) and of a carbonate ligand bound to Ru2 in molecule B (Figs. 7E).

In molecule A, a diruthenium fragment close to the side chain of Glu9A (Fig. 7C) was also found. However, the electron density is disordered and diruthenium ligands are interpreted as water molecules.

3.6. Studies of protein aggregation

Diruthenium compounds have been used as inhibitors of peptide aggregation. Indeed, it has been shown that this class of compounds can modulate the aggregation process of different beta amyloid peptide models [21,22]. To evaluate if $[Ru_2(D\text{-}p\text{-}FPhF)(O_2CCH_3)_2(O_2CO)]\cdot 3H_2O$ can act as a modulator of protein aggregation, the ability of RNase A to form dimers and higher-order oligomers was studied in the absence and in the presence of the metal compound. It is known that, when lyophilized in acetic acid, RNase A unfolds and, once dissolved in mild conditions such as phosphate buffer, it self-associates forming two domain swapped dimers (a N-terminal end swapped dimer, the N-Dimer, and a C-terminal end swapped dimer, the C-Dimer), two trimers characterized by swapping of both N- and C-termini, tetramers, pentamers and higher domain swapped oligomers [79]. Since the formation of these oligomeric species involves protein domains containing the residues here implicated in the binding of $[Ru_2(D\text{-}p\text{-}FPhF)(O_2CCH_3)_2(O_2CO)]$ fragments, we expect a partial inhibition of RNase A oligomerization prompted by the diruthenium compound. For this study, the species formed upon incubation of RNase A in acetic acid in the absence and in the presence of $[Ru_2(D\text{-}p\text{-}FPhF)(O_2CCH_3)_2(O_2CO)]$ were separated and analyzed by gel filtration chromatography (Fig. 8).

The gel filtration pattern of metalated RNase A (blue line, Fig. 8) was then compared with that of the untreated RNase A, simply dissolved in phosphate buffer and loaded on the column (black dotted line, Fig. 8) and with that of metal-free RNase A, lyophilized in acetic acid and incubated for 2 h at 37 °C (red line, Fig. 8). Results of this analysis reveal that in the presence of the diruthenium compound, the RNase A capability of forming dimers and higher-order oligomers is significantly reduced. In particular, upon lyophilization the amount of monomeric form in the protein sample in the presence of the metal complex is close to 90 %, much higher than that found for the metal-free RNase A, which is about 73 %. Furthermore, the amount of dimers formed by the protein reduces of about 50 % in the presence of $[Ru_2(D\text{-}p\text{-}FPhF)(O_2CCH_3)_2(O_2CO)]$. Regarding the trimer, its formation is quite undetectable in the presence of the metal complex, since its amount is close to 1 %, while it is about 5 % in the absence of the metal compound.

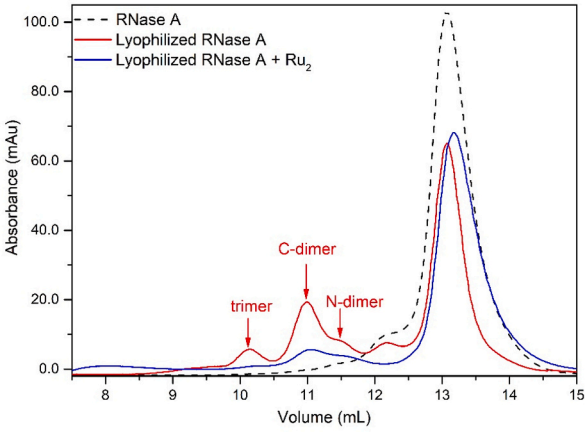

	RNase A	Lyophilized RNase A	Lyophilized RNase A + Ru_2
Monomer	99.8%	73.4%	89.4%
N-dimer	-	4.6%	2.5%
C-dimer	-	15.9%	6.7%
Trimer	-	5.9%	1.2%

Fig. 8. Gel filtration pattern on a Superdex 75 HR 10/300 of: RNase A in 0.2 M sodium phosphate buffer pH 6.7 (black dotted line), RNase A lyophilized (red line) in 40 % acetic acid and then dissolved in 0.2 M sodium phosphate buffer pH 6.7, and metalated RNase A (blue line) lyophilized in 40 % acetic acid and then dissolved in 0.2 M sodium phosphate buffer pH 6.7 in the presence of $[Ru_2(D\text{-}p\text{-}FPhF)(O_2CCH_3)_2(O_2CO)]$. In the table the percentages of monomeric and oligomeric species are reported for each RNase A sample.

4. Conclusions

Nearly sixty years after the synthesis of the first diruthenium compound, we have shown an easy synthetic route to obtain a very rare diruthenium complex with three different equatorial ligands. This compound has a neutral charge in solution, which makes it an ideal candidate to understand the protein metalation process using a neutral diruthenium compound. We have studied the physicochemical features of $[Ru_2(D\text{-}p\text{-}FPhF)(O_2CCH_3)_2(O_2CO)]\cdot 3H_2O$ and its protein binding properties using RNase A as a model system. Our combined spectroscopic/spectrometric/crystallographic approach unambiguously demonstrates that diruthenium compounds bind the protein close to His and, this particular complex can bind Glu side chains. His side chains are coordinated to the bimetallic centre at the axial site, while the Glu side chain interacts with the Ru_2 core at the equatorial site. The adduct formed upon reaction of RNase A with $[Ru_2(D\text{-}p\text{-}FPhF)(O_2CCH_3)_2(O_2CO)]\cdot 3H_2O$ retains the overall native protein conformation and presents the same thermal stability of the metal-free enzyme, but it has a reduced capability to form dimers and higher-order oligomers. The results reinforce the idea that diruthenium complexes can act as modulators of protein aggregation. This suggests the potential use of diruthenium complexes as inhibitors of amyloid peptide aggregation, as proved in some examples [21,22]. In the adduct, the formation of a highly reactive diruthenium containing species is observed, in agreement with previous observations [33,34,42].

Overall, these data expand our understanding of the reactivity of paddlewheel diruthenium complexes with proteins, providing useful information for the design of new Ru_2/peptide and Ru_2/protein adducts with potential applications ranging from catalysis to biomedicine.

CRediT authorship contribution statement

Giarita Ferraro: Writing – original draft, Investigation. **Aarón Terán:** Writing – original draft, Investigation, Data curation. **Francesco Galardo:** Investigation, Data curation. **Rosanna Lucignano:** Investigation, Data curation. **Delia Picone:** Writing – review & editing, Formal analysis. **Lara Massai:** Investigation, Data curation. **Francesca Fasulo:** Investigation, Data curation. **Ana B. Muñoz-García:** Writing – review & editing, Resources, Investigation, Formal analysis, Conceptualization. **Luigi Messori:** Writing – review & editing, Resources, Investigation, Formal analysis, Conceptualization. **Santiago Herrero:** Writing – review & editing, Resources, Investigation, Formal analysis, Conceptualization. **Antonello Merlino:** Writing – review & editing, Writing – original draft, Supervision, Resources, Formal analysis, Conceptualization.

Declaration of competing interest

The authors declare that they have no known competing financial interests or personal relationships that could have influenced the work reported in this study.

Acknowledgements

The authors thank Elettra staff for technical assistance. L.Me. and A. M. acknowledge MIUR PRIN2022 (Cod. 2022JMFC3X, "Protein Metalation by Anticancer Metal-based Drugs") for financial support. L. Me. thanks AIRC (IG-12085) for financial support. Comunidad de Madrid (Project S2017/BMD-3770-CM) and Complutense University of Madrid (GRFN32/23, GRFN24/24 and PR3/23-30828) are gratefully acknowledged for financial support. A.T. acknowledges the Complutense University for a Predoctoral Grant (CT63/19-CT64/19) and Research Stay Grant (EB25/22) and the Spanish Ministry of Science and Innovation for a Postgraduate Fellowship at Residencia de Estudiantes (2021–2022). This work was also supported by the Human Frontier Science Program (Grant number RGY0056/2022).

Appendix A. Supplementary data

Supplementary data to this article can be found online at https://doi.org/10.1016/j.ijbiomac.2024.137691.

Data availability

Data will be made available on request.

References

[1] I. Tolbatov, E. Barresi, S. Taliani, D. La Mendola, T. Marzo, A. Marrone, Inorg. Chem. Front. 10 (2023) 2226–2238.
[2] A.M. Abu-Dief, Y. Al-hawamy, A. Abdou, A.H. Alsehli, B.M. Altayeb, A. Alqurashi, G.G. Mohamed, Appl. Organomet. Chem. 38 (2024) e7637.
[3] M.S. Saddik, M.F. Al-Hakkani, A.M. Abu-Dief, M.S. Mohamed, I.A. Al-Fattah, M. Makki, M.A. El-Mokhtar, M.A. Sabet, M.S. Amin, H.A. Ahmed, K. Al-Ghamdi, M. K. Mohammad, M.H.A. Hassan, Int. J. Pharm. X 7 (2024) 100245.
[4] A.M. Abu-Dief, M.A. Said, O. Elhady, S. Alzahrani, F.S. Aljohani, T.N.A. Eskander, M.A.E.A.A. Ali El-Remaily, Inorg. Chem. Commun. 158 (2023) 111587.
[5] M. Benadiba, R.R.P. Dos Santos, D.D.O. Silva, A. Colquhoun, J. Inorg. Biochem. 104 (2010) 928–935.
[6] H.A. Al-Abdulkarim, R.M. El-khatib, F.S. Aljohani, A. Mahran, A. Alharbi, G.A. M. Mersal, N.M. El-Metwaly, A.M. Abu-Dief, J. Mol. Liq. 339 (2021) 116797.
[7] G. Ribeiro, M. Benadiba, A. Colquhoun, D. De Oliveira Silva, Polyhedron 27 (2008) 1131–1137.
[8] A. Andrade, S.F. Namora, R.G. Woisky, G. Wiezel, R. Najjar, J.A.A. Sertié, D. De Oliveira Silva, J. Inorg. Biochem. 81 (2000) 23–27.
[9] R.L.S.R. Santos, A. Bergamo, G. Sava, D. De Oliveira Silva, Polyhedron 42 (2012) 175–181.
[10] M. Benadiba, I. De, M. Costa, R.L.S.R. Santos, F.O. Serachi, D. De Oliveira Silva, A. Colquhoun, J. Biol. Inorg. Chem. 19 (2014) 1025–1035.
[11] T.E. Hanif-Ur-Rehman, R.N. Freitas, A. Colquhoun Gomes, D. De Oliveira Silva, J. Inorg. Biochem. 165 (2016) 181–191.
[12] G. Ribeiro, M. Benadiba, D. De Oliveira Silva, A. Colquhoun, Cell Biochem. Funct. 28 (2010) 15–23.
[13] E. Barresi, I. Tolbatov, T. Marzo, E. Zappelli, A. Marrone, N. Re, A. Pratesi, C. Martini, S. Taliani, F. Da Settimo, D. La Mendola, Dalton Trans. 50 (2021) 9643–9647.
[14] S.R. Alves Rico, A.Z. Abbasi, G. Ribeiro, T. Ahmed, X.Y. Wu, D. De Oliveira Silva, Nanoscale 9 (2017) 10701–10714.
[15] S.R. Alves, A. Colquhoun, X.Y. Wu, D. De Oliveira Silva, J. Inorg. Biochem. 205 (2020) 110984.
[16] S.R. Alves, R.L.S.R. Santos, B. Fornaciari, A. Colquhoun, D. De Oliveira Silva, J. Inorg. Biochem. 225 (2021) 111596.
[17] I. Coloma, J. Parrón-Ballesteros, M. Cortijo, C. Cuerva, J. Turnay, S. Herrero, Inorg. Chem. 63 (2024) 12870–12879.
[18] I. Coloma, M. Cortijo, I. Fernández-Sánchez, J. Perles, J.L. Priego, C. Gutiérrez, R. Jiménez-Aparicio, B. Desvoyes, S. Herrero, Inorg. Chem. 59 (2020) 7779–7788.
[19] I. Coloma, M. Cortijo, M.J. Mancheño, M.E. León-González, C. Gutierrez, B. Desvoyes, S. Herrero, Inorg. Chem. Front. 10 (2023) 4402–4413.
[20] G. Lozano, R. Jimenez-Aparicio, S. Herrero, E. Martinez-Salas, RNA 22 (2016) 330–338.
[21] S. La Manna, C. Di Natale, V. Panzetta, M. Leone, F.A. Mercurio, I. Cipollone, M. Monti, P.A. Netti, G. Ferraro, A. Terán, A.E. Sánchez-Peláez, S. Herrero, A. Merlino, D. Marasco, Inorg. Chem. 63 (2024) 564–575.
[22] S. La Manna, V. Panzetta, C. Di Natale, I. Cipollone, M. Monti, P.A. Netti, A. Terán, A.E. Sánchez-Peláez, S. Herrero, A. Merlino, D. Marasco, Inorg. Chem. 63 (2024) 10001–10010.
[23] M.A.S. Aquino, Coord. Chem. Rev. 248 (2004) 1025–1045.
[24] A. Terán, M. Cortijo, Á. Gutiérrez, A.E. Sánchez-Peláez, S. Herrero, R. Jiménez-Aparicio, Ultrason. Sonochem. 80 (2021) 105828.
[25] M.C. Barral, T. Gallo, S. Herrero, R. Jiménez-Aparicio, M.R. Torres, F.A. Urbanos, Chem. Eur. J. 13 (2007) 10088–10095.
[26] F.A. Cotton, A. Yokochi, Inorg. Chem. 37 (1998) 2723–2728.
[27] T. Ikeue, Y. Kimura, K. Karino, M. Iida, T. Yamaji, I. Hiromitsu, T. Sugimori, D. Yoshioka, M. Mikuriya, M. Handa, Inorg. Chem. Commun. 33 (2013) 133–137.
[28] C. Kachi-Terajima, H. Miyasaka, T. Ishii, K. Sugiura, M. Yamashita, Inorg. Chim. Acta 332 (2002) 210–215.
[29] P. Angaridis, J.F. Berry, F.A. Cotton, C.A. Murillo, X. Wang, J. Am. Chem. Soc. 125 (2003) 10327–10334.
[30] P. Angaridis, F.A. Cotton, C.A. Murillo, D. Villagrán, X. Wang, Inorg. Chem. 43 (2004) 8290–8300.
[31] A. Inchausti, A. Terán, A. Manchado-Parra, A. De Marcos-Galán, J. Perles, M. Cortijo, R. González-Prieto, S. Herrero, R. Jiménez-Aparicio, Dalton Trans. 51 (2022) 9708–9719.
[32] W.-Z. Chen, T. Ren, Inorg. Chem. 45 (2006) 8156–8164.
[33] A. Terán, G. Ferraro, A.E. Sánchez-Peláez, S. Herrero, A. Merlino, Inorg. Chem. 62 (2023) 670–674.
[34] A. Terán, G. Ferraro, P. Imbimbo, A.E. Sánchez-Peláez, D.M. Monti, S. Herrero, A. Merlino, Int. J. Biol. Macromol. 253 (2023) 126666.
[35] A. Terán, G. Ferraro, A.E. Sánchez-Peláez, S. Herrero, A. Merlino, Inorg. Chem. Front. 10 (2023) 5016–5025.
[36] L. Messori, T. Marzo, R.N.F. Sanches, Hanif-Ur-Rehman, D. de Oliveira Silva, A. Merlino, Angew. Chem. Int. Ed. 53 (2014) 6172–6175.
[37] I. Tolbatov, A. Marrone, Inorg. Chem. 61 (2022) 16421–16429.
[38] I. Tolbatov, A. Marrone, Inorg. Chim. Acta 530 (2022) 120684.
[39] A. Merlino, Chem. Commun. 57 (2021) 1295–1307.
[40] L. Messori, A. Merlino, Chem. Commun. 53 (2017) 11622–11633.
[41] L. Messori, A. Merlino, Inorg. Chem. 53 (2014) 3929–3931.
[42] A. Terán, F. Fasulo, G. Ferraro, A.E. Sánchez-Peláez, S. Herrero, M. Pavone, A. B. Muñoz-García, A. Merlino, Inorg. Chem. Front. 11 (2024) 7803–7811.
[43] R.M. Roberts, J. Organomet. Chem. 14 (1949) 277–284.
[44] R.W. Mitchell, A. Spencer, G. Wilkinson, J. Chem. Soc. Dalton Trans. (1973) 846.
[45] M.J. Frisch, G.W. Trucks, H.B. Schlegel, G.E. Scuseria, M.A. Robb, J.R. Cheeseman, G. Scalmani, V. Barone, G.A. Petersson, H. Nakatsuji, X. Li, M. Caricato, A. V. Marenich, J. Bloino, B.G. Janesko, R. Gomperts, B. Mennucci, H.P. Hratchian, J. V. Ortiz, A.F. Izmaylov, J.L. Sonnenberg, F.D. Williams-Young, F. Ding, F. Lipparini, F. Egidi, J. Goings, B. Peng, A. Petrone, T. Henderson, D. Ranasinghe, V.G. Zakrzewski, J. Gao, N. Rega, G. Zheng, W. Liang, M. Hada, M. Ehara, K. Toyota, R. Fukuda, J. Hasegawa, M. Ishida, T. Nakajima, Y. Honda, O. Kitao, H. Nakai, T. Vreven, K. Throssell, J.A. Montgomery Jr., J.E. Peralta, F. Ogliaro, M. J. Bearpark, J.J. Heyd, E.N. Brothers, K.N. Kudin, V.N. Staroverov, T.A. Keith, R. Kobayashi, J. Normand, K. Raghavachari, A.P. Rendell, J.C. Burant, S.S. Iyengar, J. Tomasi, M. Cossi, J.M. Millam, M. Klene, C. Adamo, R. Cammi, J.W. Ochterski, R.L. Martin, K. Morokuma, O. Farkas, J.B. Foresman, D.J. Fox, Gaussian 16 Rev. C.01 (2016).
[46] J. Tirado-Rives, W.L. Jorgensen, J. Chem. Theory Comput. 4 (2008) 297–306.
[47] A.V. Marenich, C.J. Cramer, D.G. Truhlar, J. Phys. Chem. B 113 (2009) 6378–6396.
[48] C. Vonrhein, C. Flensburg, P. Keller, A. Sharff, O. Smart, W. Paciorek, T. Womack, G. Bricogne, Acta Crystallogr. D Biol. Crystallogr. 67 (2011) 293–302.
[49] A.J. McCoy, R.W. Grosse-Kunstleve, P.D. Adams, M.D. Winn, L.C. Storoni, R. J. Read, J. Appl. Crystallogr. 40 (2007) 658–674.
[50] L. Vitagliano, A. Merlino, A. Zagari, L. Mazzarella, Proteins 46 (2002) 97–104.
[51] P. Emsley, K. Cowtan, Acta Crystallogr. D Biol. Crystallogr. 60 (2004) 2126–2132.
[52] G.N. Murshudov, P. Skubák, A.A. Lebedev, N.S. Pannu, R.A. Steiner, R.A. Nicholls, M.D. Winn, F. Long, A.A. Vagin, Acta Crystallogr. D Biol. Crystallogr. 67 (2011) 355–367.
[53] D. Picone, F. Donnarumma, G. Ferraro, I. Russo Krauss, A. Fagagnini, G. Gotte, A. Merlino, J. Inorg. Biochem. 146 (2015) 37–43.

[54] M. Cortijo, R. González-Prieto, S. Herrero, J.L. Priego, R. Jiménez-Aparicio, Coord. Chem. Rev. 400 (2019) 213040.
[55] Y. Sekine, W. Kosaka, H. Kano, C. Dou, T. Yokoyama, H. Miyasaka, Dalton Trans. 45 (2016) 7427–7434.
[56] S. Ngubane, K.M. Kadish, J.L. Bear, E. Van Caemelbecke, A. Thuriere, K.P. Ramirez, Dalton Trans. 42 (2013) 3571.
[57] N. Komiya, T. Nakae, H. Sato, T. Naota, Chem. Commun. (2006) 4829.
[58] W.R. Osterloh, G. Galindo, M.J. Yates, E. Van Caemelbecke, K.M. Kadish, Inorg. Chem. 59 (2020) 584–594.
[59] K. Nakamoto, Infrared and Raman Spectra of Inorganic and Coordination Compounds: Part B: Applications in Coordination, Organometallic, and Bioinorganic Chemistry, 1st edn, Wiley, 2008.
[60] A.M. Abu-Dief, O.A. Omran, M. Feizi-Dehnayebi, A. Alqurashi, I. Omar, D. Alhashmialameer, A.D.M. Mohamad, Appl. Organomet. Chem. 38 (2024) e7593.
[61] L. Messori, T. Marzo, A. Merlino, J. Inorg. Biochem. 153 (2015) 136–142.
[62] A. Inchausti, R. Mollfulleda, M. Swart, J. Perles, S. Herrero, V.G. Baonza, M. Taravillo, Á. Lobato, Adv. Sci. 11 (2024) 2401293.
[63] R. Caligiuri, L. Massai, A. Geri, L. Ricciardi, N. Godbert, G. Facchetti, M.G. Lupo, I. Rossi, G. Coffetti, M. Moraschi, E. Sicilia, V. Vigna, L. Messori, N. Ferri, G. Mazzone, I. Aiello, I. Rimoldi, Dalton Trans. 53 (2024) 2602–2618.
[64] A. Geri, S. Zineddu, L. Massai, L. Ronga, R. Lobinski, J. Gailer, L. Messori, J. Inorg. Biochem. 252 (2024) 112479.
[65] G. Ferraro, N. Demitri, L. Vitale, G. Sciortino, D. Sanna, V. Ugone, E. Garribba, A. Merlino, Inorg. Chem. 60 (2021) 19098–19109.
[66] I. Russo Krauss, L. Messori, M.A. Cinellu, D. Marasco, R. Sirignano, A. Merlino, Dalton Trans. 43 (2014) 17483–17488.
[67] G. Ferraro, A. Pratesi, L. Messori, A. Merlino, Dalton Trans. 49 (2020) 2412–2416.
[68] M. Caterino, A.A. Petruk, A. Vergara, G. Ferraro, D. Marasco, F. Doctorovich, D. A. Estrin, A. Merlino, Dalton Trans. 45 (2016) 12206–12214.
[69] R.T. Raines, Chem. Rev. 98 (1998) 1045–1066.
[70] D. Loreto, B. Maity, T. Morita, H. Nakamura, A. Merlino, T. Ueno, Inorg. Chem. 62 (2023) 7515–7524.
[71] G. Ferraro, T. Lyčková, L. Massai, P. Štarha, L. Messori, A. Merlino, Dalton Trans. 53 (2024) 8535–8540.
[72] G. Ferraro, T. Marzo, M.E. Cucciolito, F. Ruffo, L. Messori, A. Merlino, Int. J. Mol. Sci. 20 (2019) 520.
[73] J. Hildebrandt, H. Görls, N. Häfner, G. Ferraro, M. Dürst, I.B. Runnebaum, W. Weigand, A. Merlino, Dalton Trans. 45 (2016) 12283–12287.
[74] N. Pontillo, G. Ferraro, L. Messori, G. Tamasi, A. Merlino, Dalton Trans. 46 (2017) 9621–9629.
[75] A. Annunziata, M.E. Cucciolito, M. Di Ronza, G. Ferraro, M. Hadiji, A. Merlino, D. Ortiz, R. Scopelliti, F. Fadaei Tirani, P.J. Dyson, F. Ruffo, Organometallics 42 (2023) 952–964.
[76] G. Ferraro, A.M. Mansour, A. Merlino, Dalton Trans. 47 (2018) 10130–10138.
[77] Đ. Miodragović, A. Merlino, E.P. Swindell, A. Bogachkov, R.W. Ahn, S. Abuhadba, G. Ferraro, T. Marzo, A.P. Mazar, L. Messori, T.V. O'Halloran, J. Am. Chem. Soc. 141 (2019) 6453–6457.
[78] N. Borkakoti, Eur. J. Biochem. 132 (1983) 89–94.
[79] G. Gotte, D.V. Laurents, A. Merlino, D. Picone, R. Spadaccini, FEBS Lett. 587 (2013) 3601–3608.